Electronic Supplementary Material (ESI) for Journal of Materials Chemistry A.

Supporting Information

FeP_3 Monolayer as High-Efficiency Catalysts for Hydrogen Evolution Reaction

Shuang Zheng, Tong Yu, Jianyan Lin, Huan Lou, Haiyang Xu, and Guochun Yang*

Centre for Advanced Optoelectronic Functional Materials Research and Key Laboratory for UV Light-Emitting Materials and Technology of Ministry of Education, Northeast Normal University, Changchun 130024, China

Index **Page**

1. Computational details……………………………………………………2

2. Electron localization function of the FeP_x monolayers………………………4

3. The P_2 and P_4 units are alternate arrangement through Fe-P bonding of FeP_3 monolayer……………………………………………………………………4

4. Relative formation energy of the FeP_x monolayers……………………………5

5. Dynamical stability of the FeP_x monolayers ……………………………………5

6. Thermal stability of the FeP_x monolayers………………………………………6

7. Projected density of states of the FeP_x monolayers……………………………7

8. Hydrogen adsorption and calculated Gibbs free energies at different sites for the FeP_x monolayers……………………………………………………………………8

9. The structure of the FeP_x monolayer with hydrogen adsorption………………9

10. The Gibbs free energies of FeP_x under biaxial strain…………………………14

11. Structural information of predicted FeP_x monolayers…………………………15

12. Bader charge analysis of the FeP_x monolayers…………………………………16

13. References……………………………………………………………………17

Computational Details

The particle swarm optimization (PSO) method within the evolutionary algorithm as implemented in the Crystal structure AnaLYsis by Particle Swarm Optimization (CALYPSO) code[1,2] was employed to find the lowest energy structures of FeP_x (x = 1-4) monolayers. Unit cells containing 1, 2, and 4 formula units (f.u.), including buckled and planar structures, were considered. In the first step, random structures with certain symmetry are constructed in which atomic coordinates are generated by the crystallographic symmetry operations. Local optimizations using the VASP code[3] were done with the conjugate gradients method and stopped when Gibbs free energy changes became smaller than 1×10^{-6} eV per cell. After processing the first generation structures, 60% of them with lower enthalpies are selected to construct the next generation structures by Particle Swarm Optimization (PSO). 40% of the structures in the new generation are randomly generated. A structure fingerprinting technique of bond characterization matrix is applied to the generated structures, so that identical structures are strictly forbidden. These procedures significantly enhance the diversity of the structures, which is crucial for structural global search efficiency. In most cases, structural searching simulations for each calculation were stopped after generating 1000 ~ 1200 structures (e.g., about 20 ~ 30 generations).

The local structural relaxations and electronic properties calculations were performed in the framework of the density functional theory (DFT)[4] within the generalized gradient approximation (GGA)[5] as implemented in the VASP code. The $3d^7 4s^1$, and $3s^2 3p^3$ atomic orbitals were treated as valence states for Fe, and P respectively. The cut-off energy for the expansion of wavefunctions into plane waves is set to 450 eV in all calculations. Phonon calculations were performed by using a supercell approach with the finite displacement method[6] as implemented in the Phonopy code.[7] Dependent on specific structures of stable monolayers, different supercells are used: 3 × 3 × 1 for FeP with $P4/nmm$ symmetry, 1 × 4 × 1 for FeP_2 with $C2/m$ symmetry, 2 × 2 × 1 for FeP_3 with $C2/m$ symmetry, and 3 × 2 × 1 for FeP_4 with Pm symmetry. Among the predicted stable structures, the FeP with $P4/nmm$

symmetry is the most stable. First-principles molecular dynamics (MD)[8] simulations for a large supercell were performed at different temperatures of 500 K. The supercells adopt 5 × 5 × 1 for FeP with *P*4/*nmm* symmetry, 1 × 7 × 1 for FeP_2 with *C*2/*m* symmetry, 2 × 3 × 1 for FeP_3 with *C*2/*m* symmetry, and 4 × 4 × 1 for FeP_4 with *Pm* symmetry. MD simulation in NVT ensemble lasted for 10 ps with a time step of 1.0 fs. The temperature was controlled by using the Nosé-Hoover method.

Cohesive energy

Cohesive energy is widely used to ascertain the feasibility for experimental synthesis of the predicted 2D materials. Here, the cohesive energy E_{coh} is calculated based on the equation of $E_{coh} = (E_{Fe} + x \times E_P - E_{FeP_x})/(x+1)$, where E_{Fe}, E_P, and E_{FeP_x} are the energies of Fe, P atom, and 2D FeP_x unit cell, respectively.

Supporting Figures

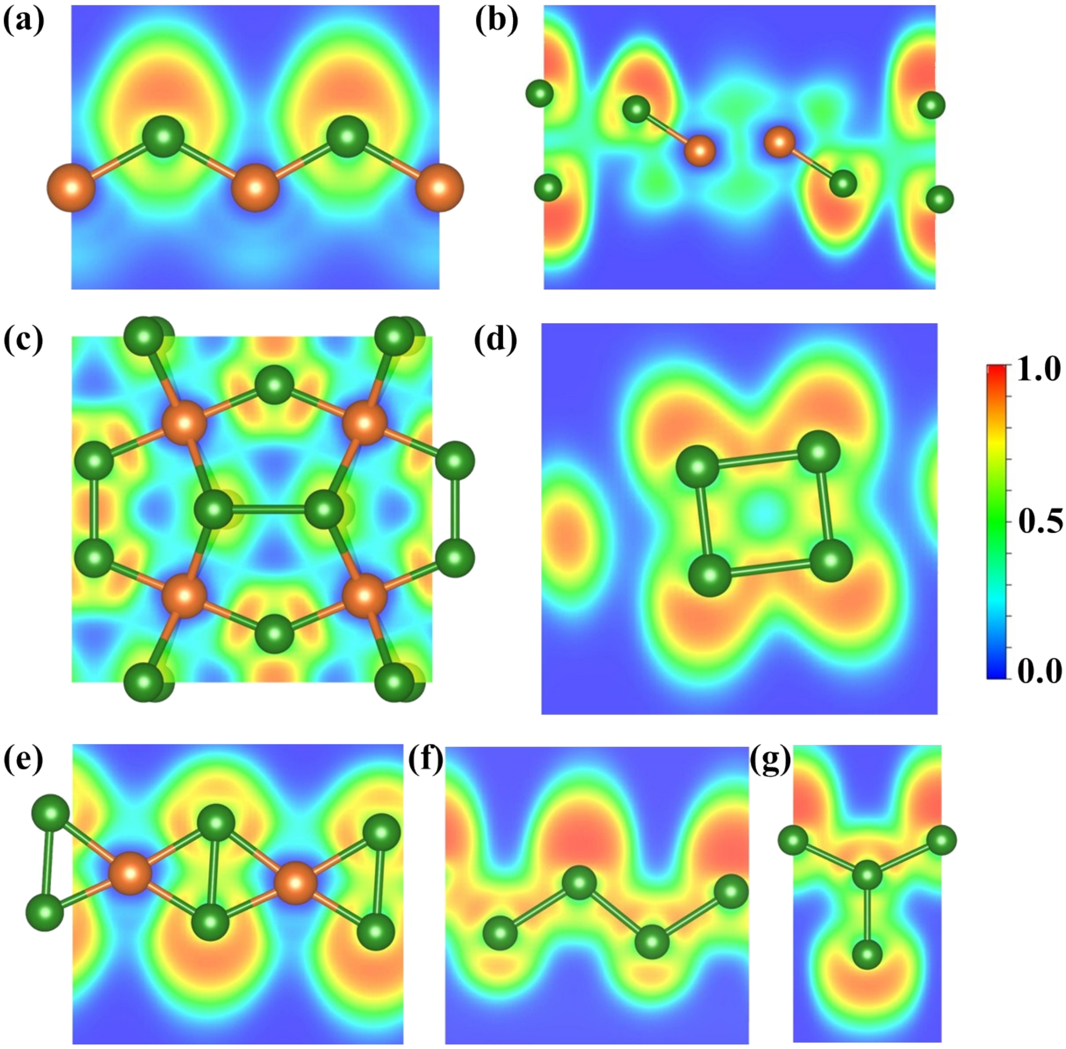

Figure. S1 ELF map of the (a) FeP monolayer, (b) FeP_2 monolayer, (c) - (d) FeP_3 monolayer, and (e) - (f) FeP_4 monolayer.

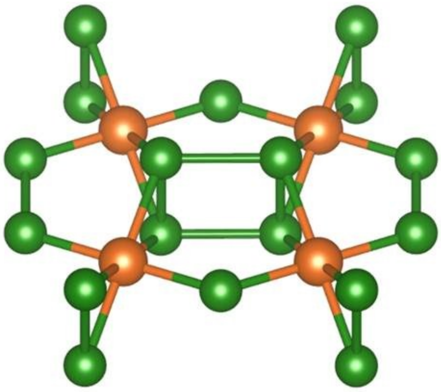

Figure. S2 The P_2 and P_4 units are alternate arrangement through Fe-P bonding of FeP_3 monolayer.

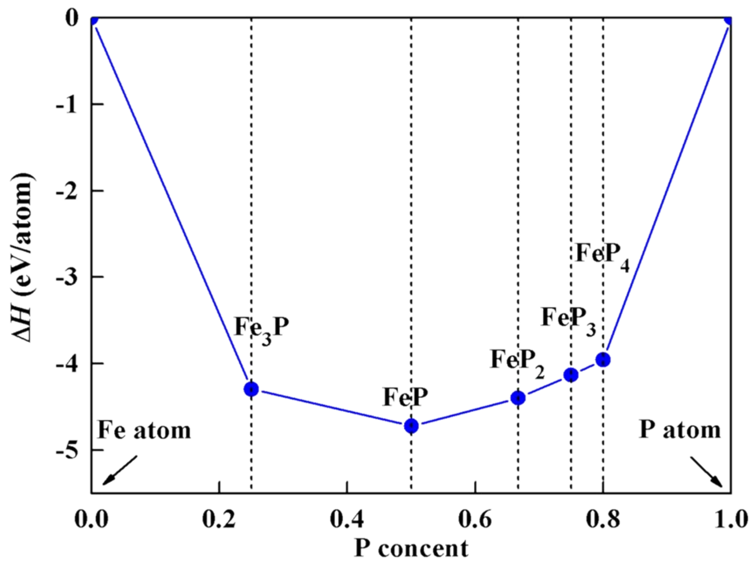

Figure. S3 Relative formation energy of FeP_x monolayers with respect to Fe, P atoms and the Fe_3P monolayer.[9]

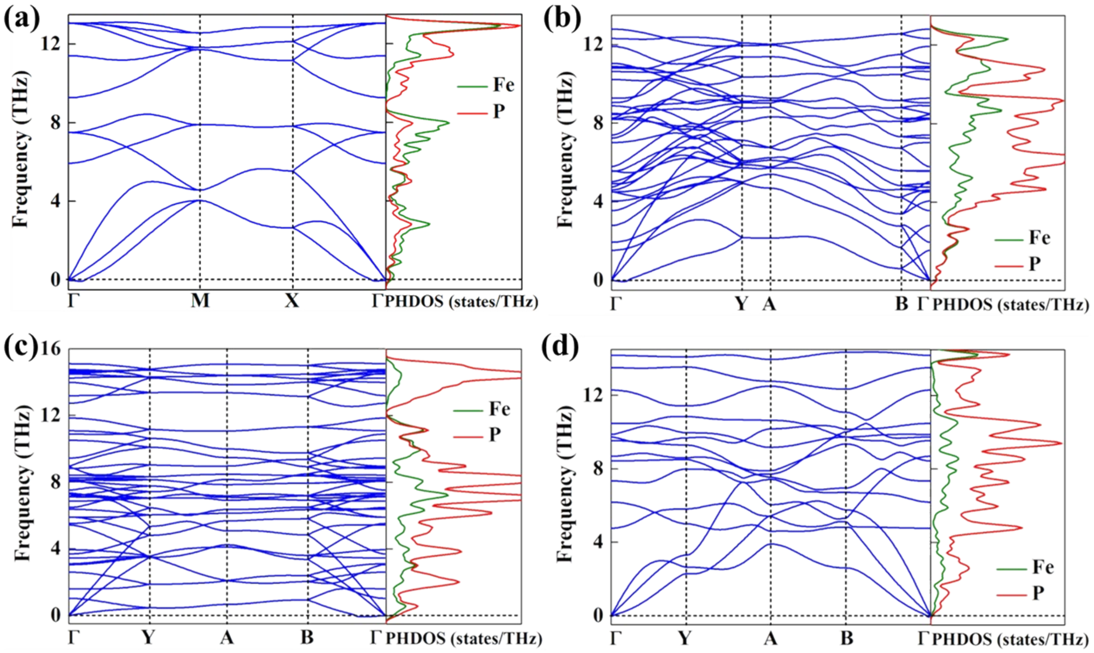

Figure. S4 Phonon dispersive curves and projected phonon density of states (PHDOS) of the (a) FeP monolayer, (b) FeP_2 monolayer, (c) FeP_3 monolayer, and (d) FeP_4 monolayer.

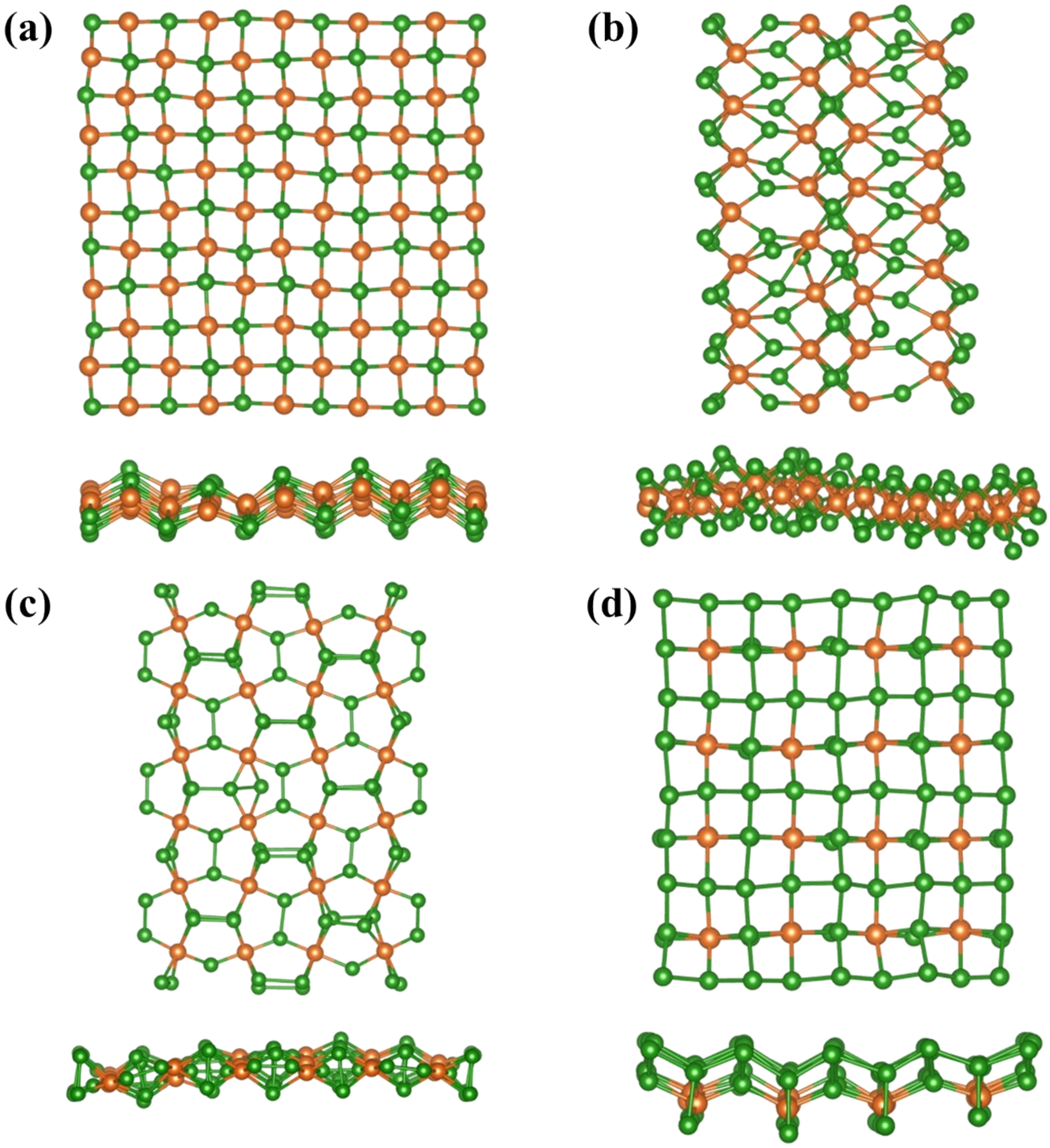

Figure. S5 Snapshots of the final frame of (a) FeP, (b) FeP_2, (c) FeP_3, and (d) FeP_4 monolayer at time of 10 ps during AIMD simulations under the temperatures of 500 K.

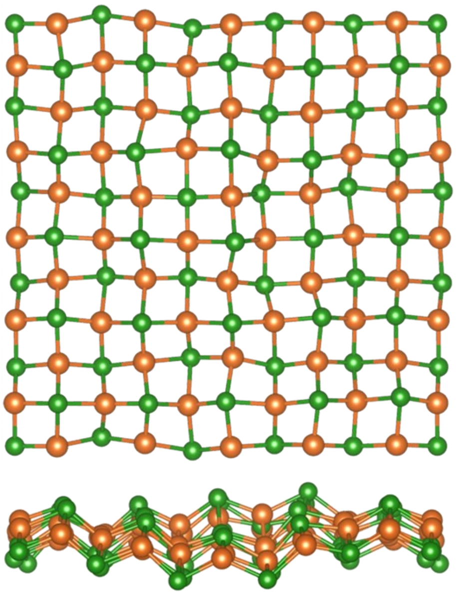

Figure. S6 Snapshots of the final frame of FeP monolayer at time of 10 ps during AIMD simulations under the temperatures of 1000 K.

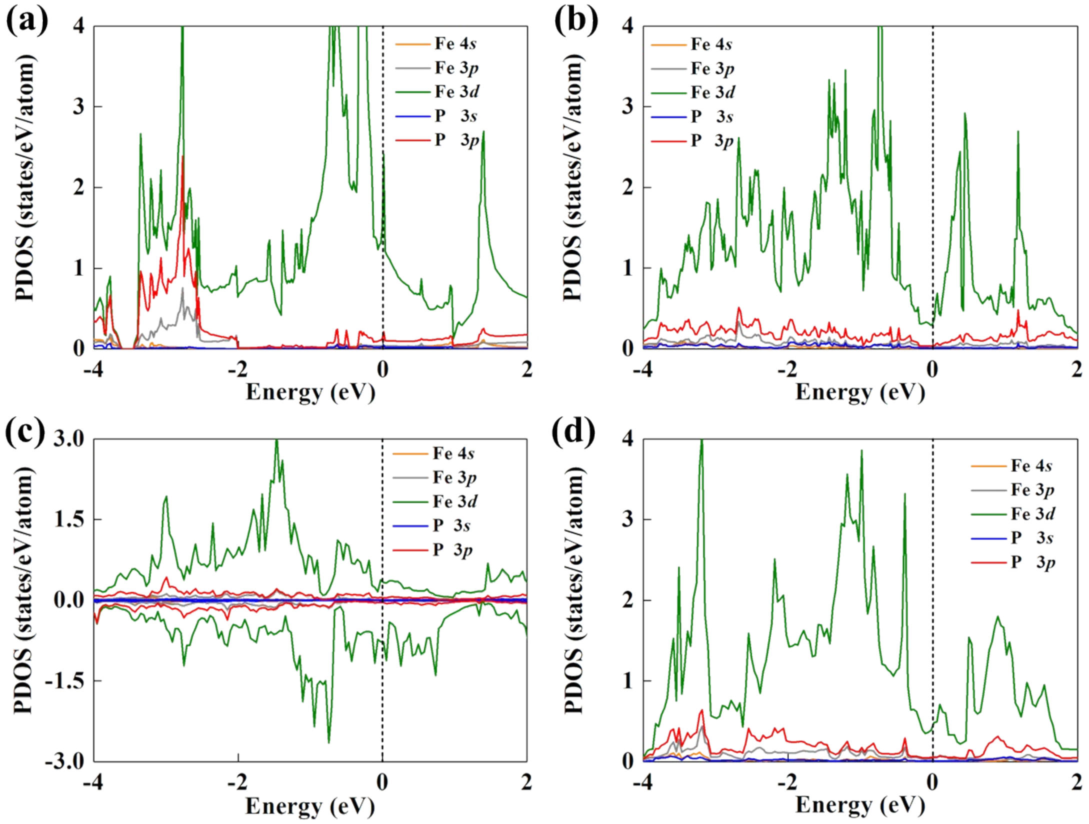

Figure. S7 Projected density of states (PDOS) for (a) FeP monolayer, (b) FeP_2 monolayer, (c) FeP_3 monolayer, and (d) FeP_4 monolayer.

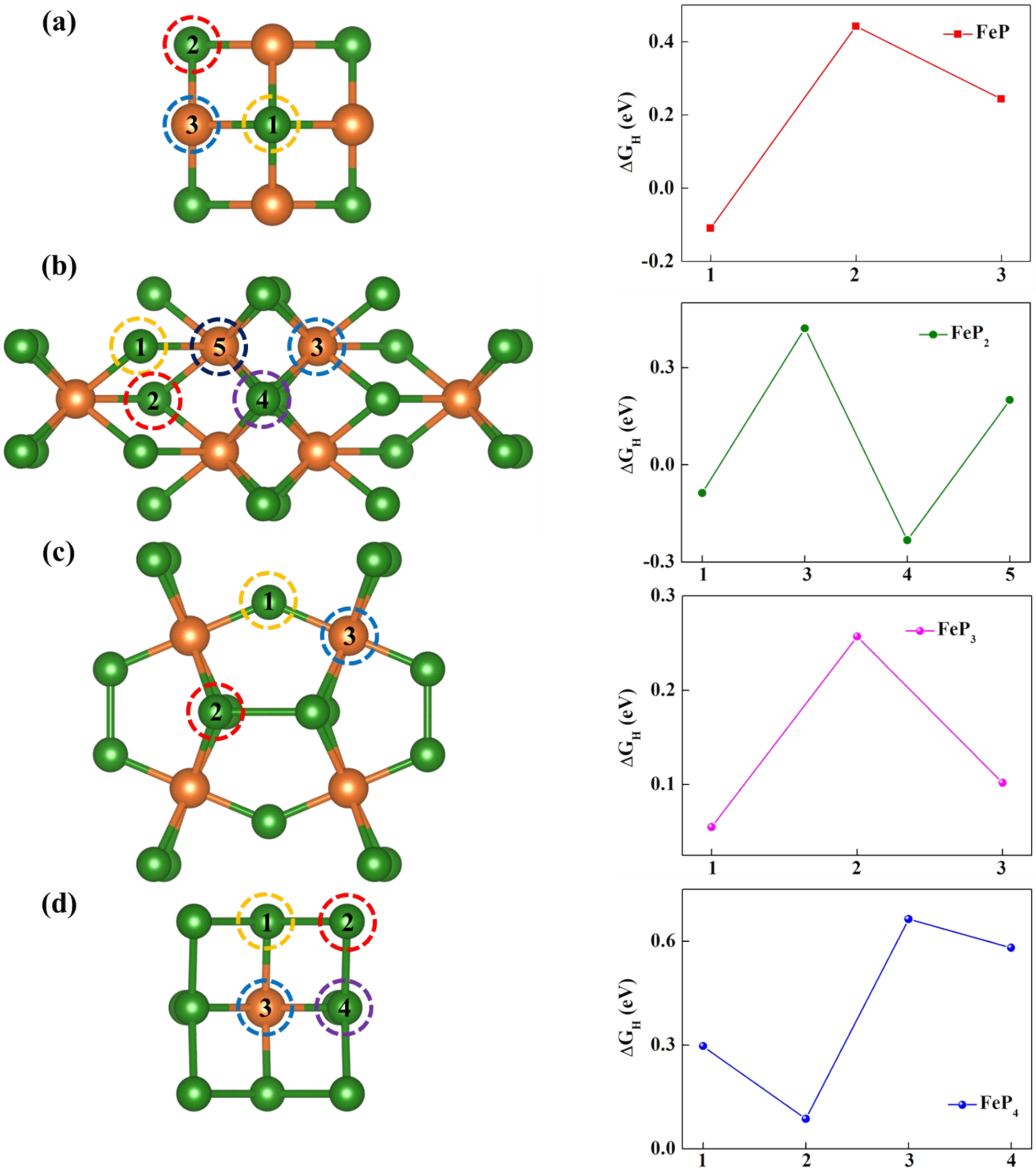

Figure. S8 Hydrogen adsorption and calculated Gibbs free energies at different sites for the (a) FeP monolayer, (b) FeP_2 monolayer, (c) FeP_3 monolayer, and (d) FeP_4 monolayer. The FeP_2 monolayer destroy when hydrogen adsorption at 2 site.

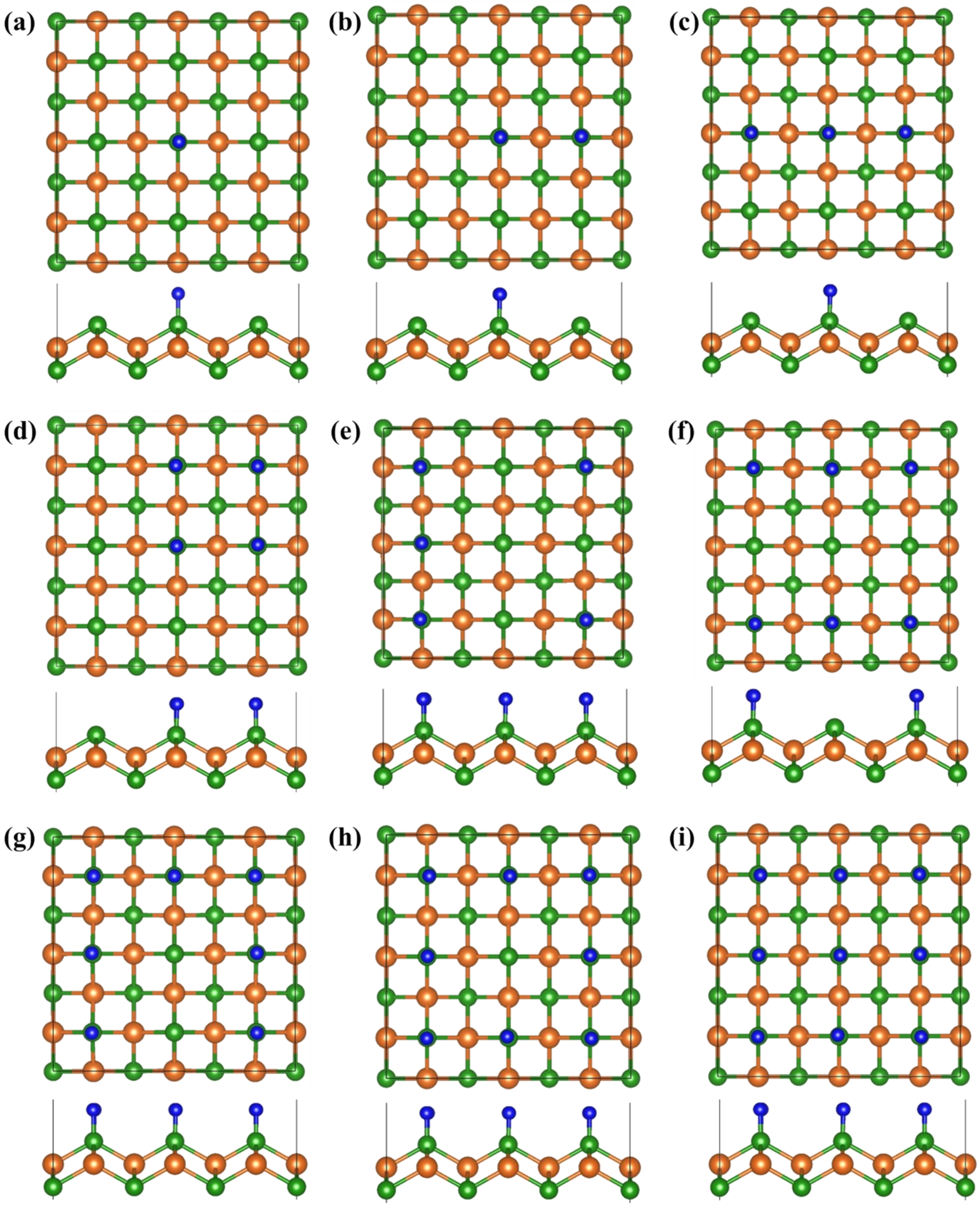

Figure. S9 Top and side views of the structure of the FeP monolayer with hydrogen adsorption. The different H coverages can be simulated with an increment of 1/9.

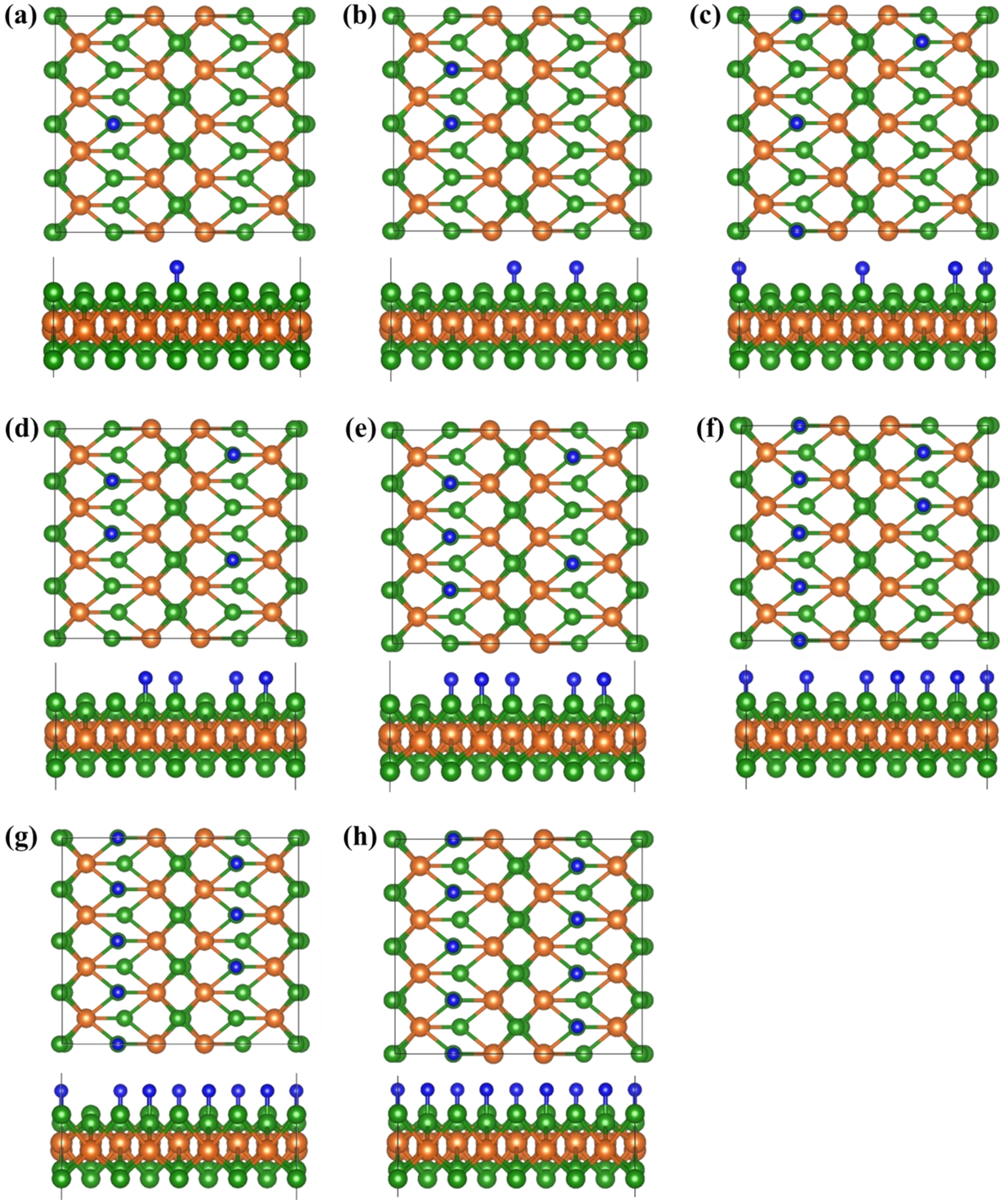

Figure. S10 Top and side views of the structure of the FeP$_2$ monolayer with hydrogen adsorption. The different H coverages can be simulated with an increment of 1/8.

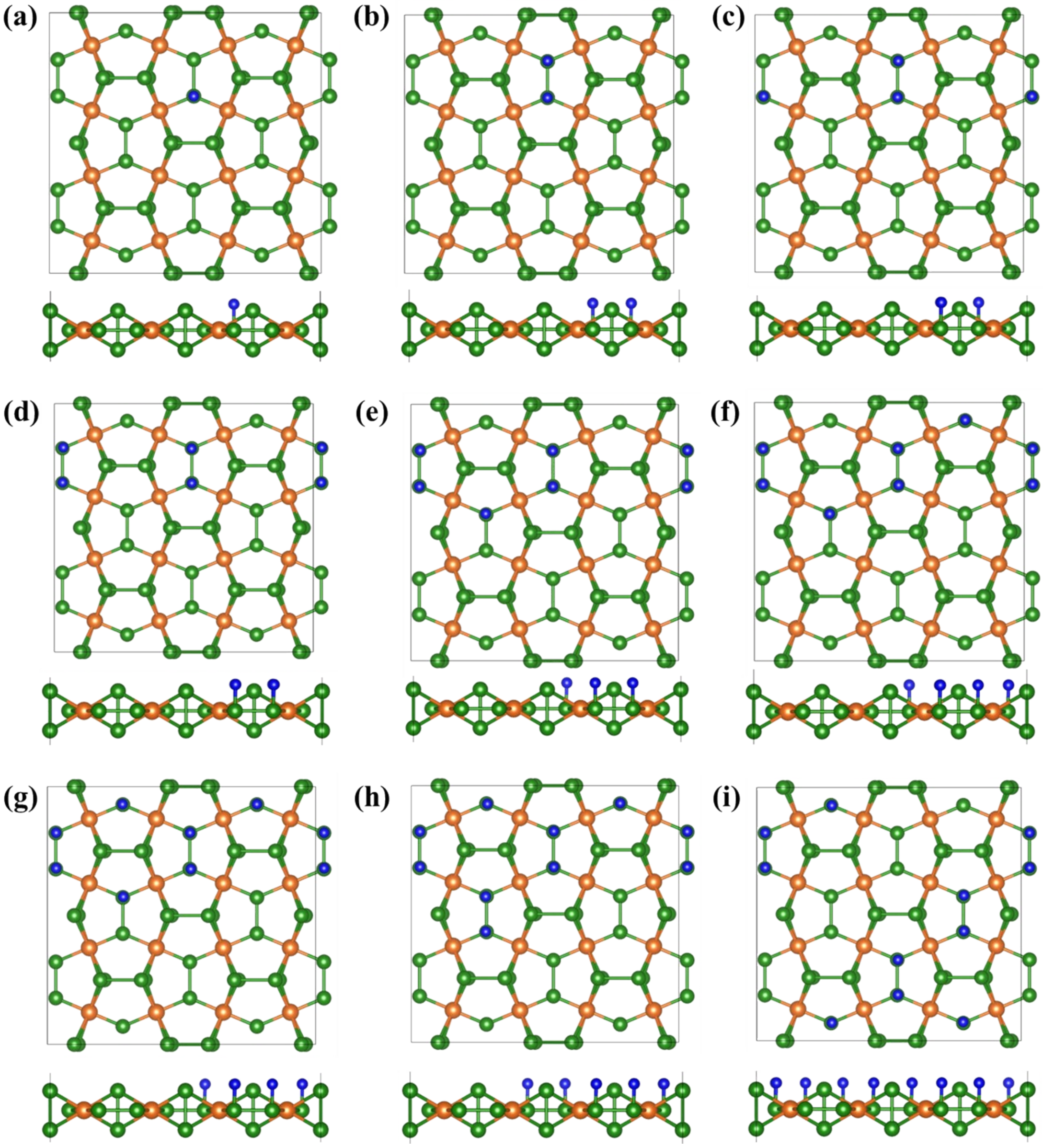
(a)
(b)
(c)
(d)
(e)
(f)
(g)
(h)
(i)

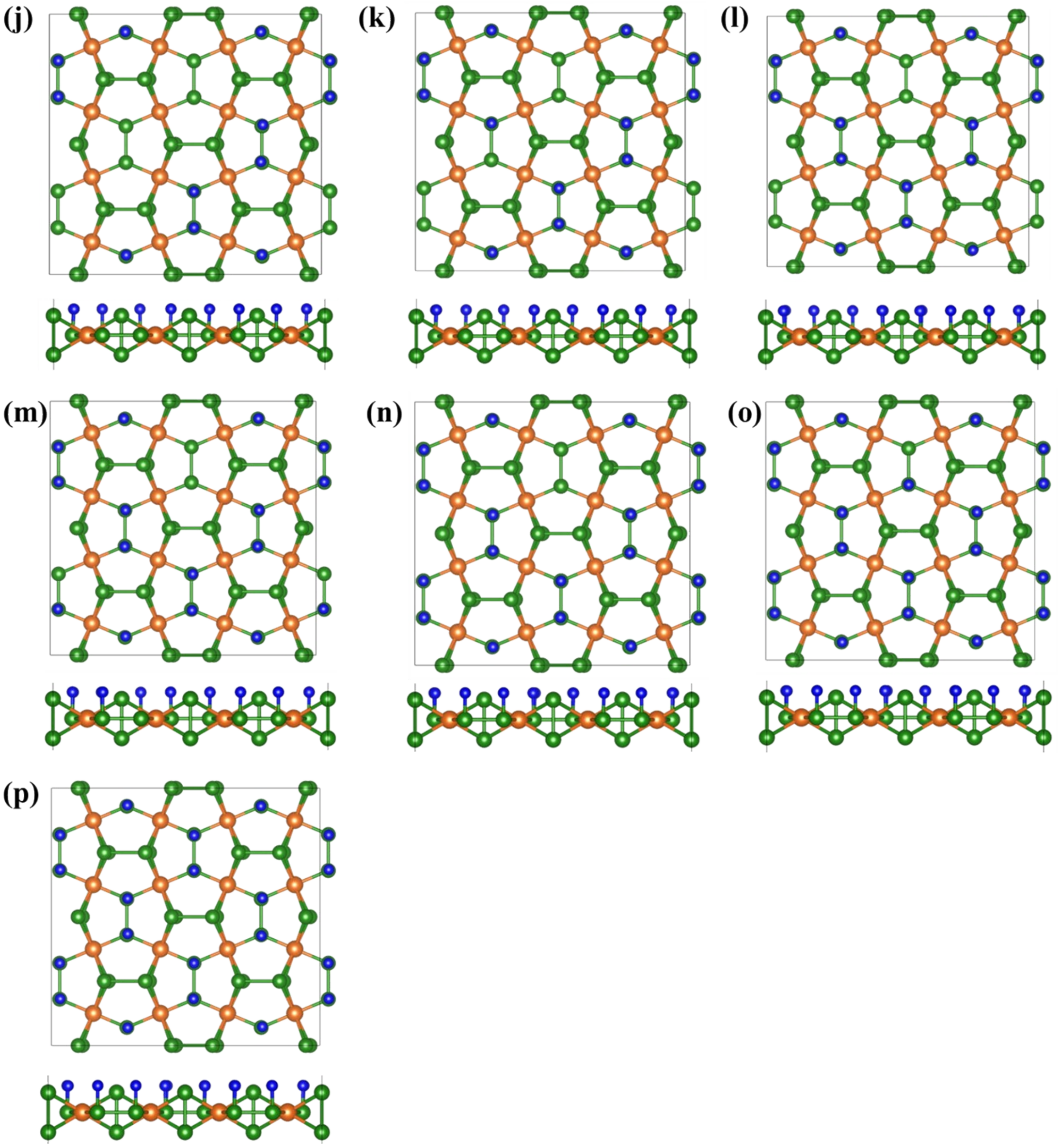

Figure. S11 Top and side views of the structure of the FeP_3 monolayer with hydrogen adsorption. The different H coverages can be simulated with an increment of 1/16.

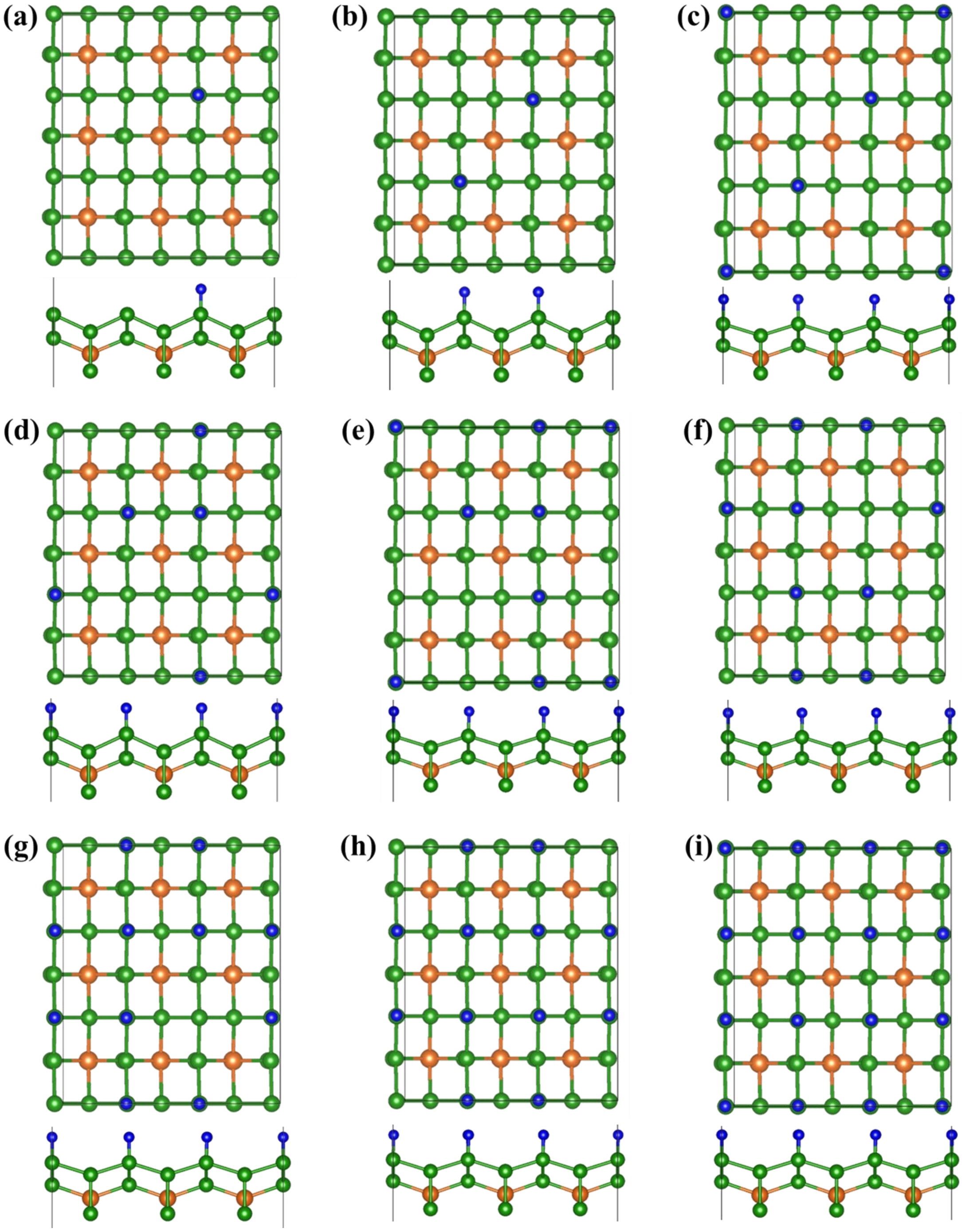

Figure. S12 Top and side views of the structure of the FeP_4 monolayer with hydrogen adsorption. The different H coverages can be simulated with an increment of 1/9.

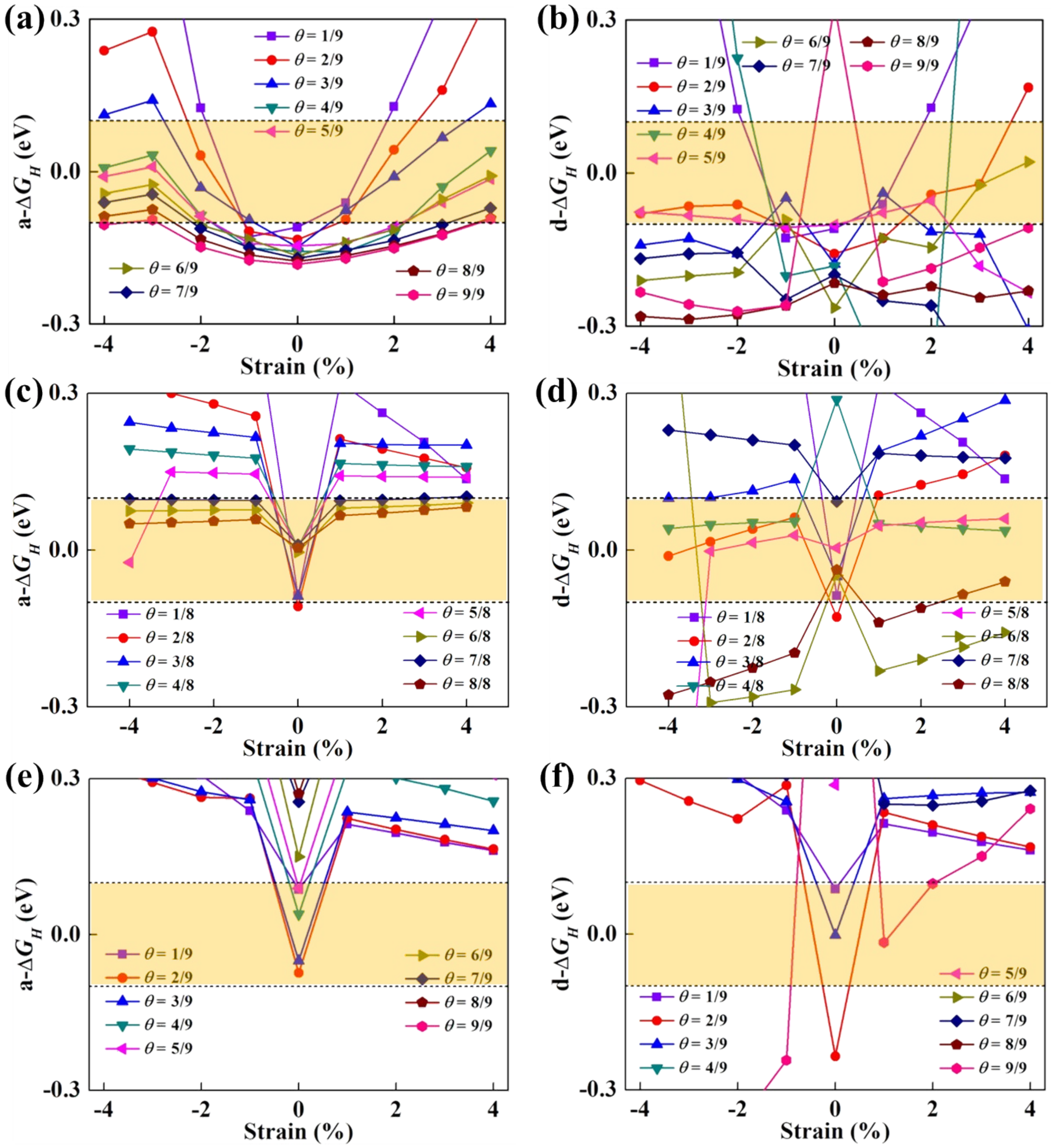

Figure. S13 The Gibbs free energies under biaxial strain for FeP (a) a-ΔG_H, (b) d-ΔG_H; for FeP_2 (c) a-ΔG_H, (d) d-ΔG_H; for FeP_4 (e) a-ΔG_H, (f) d-ΔG_H.

Supporting Tables

Table S1 Detailed structural information of the predicted stable FeP_x monolayers.

Phase	Space Group	Lattice Parameters (Å, °)	Wyckoff Positions (fractional) Atoms	*x*	*y*	*z*
FeP	*P*4/*nmm*	$a = 3.73020$	Fe(2b)	1.00000	0.00000	0.50000
		$b = 3.73020$	P(2c)	0.50000	0.00000	0.45450
		$c = 23.90970$				
		$\alpha = \beta = \gamma = 90.000$				
FeP_2	*C*2/*m*	$a = 12.13140$	Fe(4i)	0.89830	0.50000	0.49280
		$b = 2.62750$	P(4i)	0.73576	0.50000	0.54650
		$c = 22.85930$	P(4i)	0.01034	0.00000	0.43575
		$\alpha = \gamma = 90.000$				
		$\beta = 91.5487$				
FeP_3	*C*2/*m*	$a = 7.91300$	Fe(4f)	0.25000	0.25000	0.50000
		$b = 7.52210$	P(4i)	0.33197	0.50000	0.54798
		$c = 22.69210$	P(4i)	0.36340	0.50000	0.45138
		$\alpha = \gamma = 90.000$	P(4h)	0.50000	0.13999	0.50000
		$\beta = 83.340$				
FeP_4	*Pm*	$a = 3.74680$	Fe(1b)	0.34831	0.50000	0.47196
		$b = 4.20240$	P(1b)	0.83283	0.50000	0.42797
		$c = 22.83070$	P(1b)	0.86791	0.50000	0.52770
		$\alpha = \gamma = 90.000$	P(1a)	0.88318	0.00000	0.57110
		$\beta = 93.3094$	P(1a)	0.36214	0.00000	0.51128

Table S2 Bader charge analysis of the FeP_x monolayers.

Phase	Atom	Charge
FeP	Fe	0.30
	P	-0.30
FeP_2	Fe	0.20
	P1	-0.12
	P2	0.08
FeP_3	Fe	0.33
	P1	-0.08
	P2	-0.10
	P3	-0.15
FeP_4	Fe	0.24
	P1	-0.02
	P2	-0.02
	P3	-0.16
	P4	-0.04

References

1 Y. Wang, J. Lv, L. Zhu and Y. Ma, *Comput. Phys. Commun.*, 2012, **183**, 2063–2070.

2 Y. Wang, J. Lv, L. Zhu and Y. Ma, *Phys. Rev. B Condens. Matter Mater. Phys.*, 2010, **82**, 094116.

3 G. Kresse and J. Furthmu, *Phys. Rev. B.*, 1996, **54**, 11169–11186.

4 W. KOHN and L. J. SHAM, *Phys. Rev*, 1965, **140**, A1133–A1138.

5 J. P. Perdew, K. Burke and M. Ernzerhof, *Phys. Rev. Lett.*, 1996, **77**, 3865–3868.

6 K. Parlinski, Z. Q. Li and Y. Kawazoe, *Phys. Rev. Lett.*, 1997, **78**, 4063–4066.

7 A. Togo, F. Oba and I. Tanaka, *Phys. Rev. B - Condens. Matter Mater. Phys.*, 2008, **78**, 134106.

8 G. J. Martyna, M. L. Klein and M. Tuckerman, *J. Chem. Phys.*, 1992, **97**, 2635–2643.

9 S. Zheng, C. Huang, T. Yu, M. Xu, S. Zhang, H. Xu, Y. Liu, E. Kan, Y. Wang and G. Yang, *J. Phys. Chem. Lett.*, 2019, **10**, 2733–2738.